Li *et al.*
Chinese Journal of Mechanical Engineering (2022) 35:86
https://doi.org/10.1186/s10033-022-00757-6

Chinese Journal of Mechanical Engineering

ORIGINAL ARTICLE Open Access

Influence of Piston Number on Churning Losses in Axial Piston Pumps

Ying Li[1,2], Xing Chen[1], Hao Luo[1], Junhui Zhang[2] and Jin Zhang[1*]

Abstract

Raising the rotational speed of an axial piston pump is useful for improving its power density; however, the churning losses of the piston increase significantly with increasing speed, and this reduces the performance and efficiency of the axial piston pump. Currently, there has been some research on the churning losses of pistons; however, it has rarely been analyzed from the perspective of the piston number. To improve the performance and efficiency of the axial piston pump, a computational fluid dynamics (CFD) simulation model of the churning loss was established, and the effect of piston number on the churning loss was studied in detail. The simulation analysis results revealed that the churning losses initially increased as the number of pistons increased; however, when the number of pistons increased from six to nine, the torque of the churning losses decreased because of the hydrodynamic shadowing effect. In addition, in the analysis of cavitation results, it was determined that the cavitation area of the axial piston pump was mainly concentrated around the piston, and the cavitation became increasingly severe as the speed increased. By comparing the simulation results with and without the cavitation model, it was observed that the cavitation phenomenon is beneficial for the reduction of churning losses. In this study, a piston churning loss test rig that can eliminate other friction losses was established to verify the accuracy of the simulation results. A comparative analysis indicated that the simulation results were consistent with the actual situation. In addition, this study also conducted a simulation study on seven and nine piston pumps with the same displacement. The simulation results revealed that churning losses of the seven pistons were generally greater than those of the nine pistons under the same displacement. In addition, regarding the same piston number and displacement, reducing the pitch circle radius of piston bores is effective in reducing the churning loss. This research analyzes the effect of piston number on the churning loss, which has certain guiding significance for the structural design and model selection of axial piston pumps.

Keywords: Axial piston pumps, Churning losses, Pistons, CFD simulations, Experimental study

1 Introduction

The hydraulic pump is the most important power source of the hydraulic system, which is equivalent to the "heart" of the hydraulic system. The performance of a hydraulic system is largely dependent on its hydraulic pump. Among various types of hydraulic pumps, axial piston pumps have some inherent advantages, such as negligible size, high efficiency, smooth operation, easy displacement control, and high-limit operating parameters. Therefore, axial piston pumps are approximately always utilized as an oil source in important fields such as modern engineering machinery and aerospace [1–4]. With the increasing demand for energy conservation worldwide, it is necessary to further improve the efficiency of hydraulic systems, and this can be done by improving the efficiency of a hydraulic pump.

Generally, the energy losses caused by the axial piston pump during operation can be divided into three parts. The first, second, and third parts are volume, mechanical,

*Correspondence: zhangjin@ysu.edu.cn

[1] School of Mechanical Engineering, Yanshan University, Qinhuangdao 066004, China
Full list of author information is available at the end of the article

and churning losses, respectively [5–9]. Compared with studies on mechanical and volumetric losses, there are few studies on churning losses. The churning losses of axial piston pumps are usually not valued. This is because the speed of the pump is generally less than 3000 r/min, and the effect of churning losses on the pump is negligible. However, in the aerospace and other fields, it is necessary to increase the speed to improve the power density of the pump. However, hydraulic oil is also stirred by the piston and cylinder block at a high speed with an increase in the rotating speed. In this case, the flow velocity of the oil in the casing of the axial piston pump will increase rapidly. At this time, the churning loss significantly increases, and directly affects the performance and life of the axial piston pump [10, 11]. The churning losses caused by rotating pistons and cylinder blocks in axial piston pumps have been studied over the past decades. Jang [12] first studied the theory of churning losses in axial piston pumps and established a simplified churning loss model. He stated that the rotary motion of the piston had a significant effect on churning losses. Parker [13] added a power booster to the piston motor, which modifies the flow of oil to reduce churning losses. The experimental results reveal that the power booster can increase the motor power by 10% when the rotation speed reaches 9000 r/min. Enekes [14] conducted a detailed computational fluid dynamics (CFD) simulation study on the churning losses of high-speed axial piston pumps. They established a CFD simulation model of the churning losses under hydraulic oils of different viscosities and experimentally verified the effect of these oils on the churning losses. Zecchi et al. [15] considered the effect of Reynolds number on churning losses and further perfected the concentrated parameter model of piston churning losses. In an experimental study of the churning losses of an axial piston pump, cavitation occurred when the fluid flowed outside the piston. Moreover, owing to cavitation, the flow resistance between pistons was reduced [16]. Hasko et al. [17] measured the power loss value of an axial piston pump with a size of 52 cm^3/r via experiments. In this study, the axial piston pump was adjusted to a zero displacement to measure the torque at different rotating speeds. This process was then repeated under dry conditions. The function of churning loss with rotation speed was obtained by calculating the difference between the dry and wet pumps.

The piston is one of the main factors that affect the churning loss of an axial piston pump. Jang [12] and Zecchi et al. [15] conducted research on the churning losses of pistons. In addition, most research on the number of pistons focused on flow pulsation. Jeong and Kim [18] derived an equation for estimating the average frictional moment loss of a piston. Under the same conditions, the equation assumed that the average piston friction moment increases with the number of pistons: Constantly altering the angle of the swash plate to resist torque fluctuations can effectively reduce the pump noise level [19]. They established a mathematical model to derive the torque equation acting on the input shaft, which is a function of the torque and number of pistons. In addition, the odd and even numbers of pistons have been extensively studied, and their torque component formulas on the high-pressure and low-pressure sides have been obtained, respectively. In a simulation study of an aviation pump, the pressure drop performance was observed by studying the rotary pressure, and the influence of the number of pistons on the pressure drop was analyzed [20]. They simulated the pump outlet pressure using two pump models with the same displacement of nine and 11 pistons. The results indicated that the control valve must be redesigned if the number of pistons changes. Ling et al. [21] proposed a new double-acting piston pump to improve the pulsation performance of a swash plate piston pump, and analyzed the impact of the number of pistons on the flow pulsation rate.

The above analysis studied the churning losses caused by the rotation of the multi-pistons and influence of the number of pistons on the flow pulsation in axial piston pumps. However, few researchers have analyzed the effect of churning loss from the perspective of piston number. It is well known that the churning losses of the piston increase significantly with an increase in pump speed. Therefore, the development of a high-performance aviation piston pump is one of the challenges that should be addressed. However, owing to the complex dynamic characteristics and various forms of energy consumption in the axial piston pump, the mechanism of churning losses and its reduction measures have not been fully studied. In this study, churning losses were analyzed from the perspective of the number of pistons. First, a CFD simulation of different numbers of axial piston pumps was conducted, and simulation results were verified using a special test rig that can separate other energy consumption effects. In addition, we conducted simulation studies on the same displacement pump with seven and nine pistons.

2 CFD Simulation

With the rapid development of computers, computational fluid dynamics (CFD) simulation technology has exhibited unique advantages in various fields. In particular, when studying the flow challenge of complex flow fields, the utilization of CFD simulation technology has a lower cost and shorter cycle time than a physical prototype test, and the calculation accuracy can meet the engineering requirements, which has become an important

method of flow field analysis [22, 23]. The CFD simulation technology has been widely employed in engineering [24–26]. Computational fluid dynamics models based on the Navier-Stokes equation are widely utilized to solve the motion characteristics of fluids in hydraulic pumps. The vector expression of the Navier-Stokes equation is as follows:

$$\rho\frac{\mathrm{d}\boldsymbol{V}}{\mathrm{d}t}=\rho g-\nabla p+\mu\nabla^2\boldsymbol{V}, \tag{1}$$

where $\boldsymbol{V}$ is the velocity vector of the fluid, t is time, ρ is fluid density, g is gravitational acceleration, p is pressure, and the constant μ is the dynamic viscosity coefficient.

Currently, some commercial software packages are utilized by researchers to build CFD models of piston pumps. Because this research is aimed at the cavitation of the piston area and churning losses during the operation of the axial piston pump, compared with other common CFD software, Pumplinx has great advantages in dynamic mesh generation and cavitation prediction. In addition, Pumplinx employs an accurate and intuitive dynamic grid method to process pump movement. Therefore, Pumplinx was utilized as the calculation tool in this study.

2.1 CFD Modeling

In the axial piston pump, mechanical energy is converted into hydraulic energy via telescopic motion of the piston. To study the churning losses, we are first required to establish an axial piston pump model with a uniform cylinder elongation outside the cylinder of the piston-slipper assembly. To control the number of pistons as the only variable, the length of the piston-slipper assembly outside the cylinder block in this model remains the same, and the displacement of the axial piston pump is zero at this time. This is because on the one hand, the friction loss cannot be peeled off when the piston reciprocates; on the other hand, it is also verified by the test bench that the piston extension is fixed. Simultaneously, to avoid friction between the central spline of the cylinder and main shaft, piston and cylinder, and piston and slipper, the cylinder and main shaft are processed into an integrated structure, and the slipper and piston are designed as an integrated structure. In addition, the structure of the swash plate is eliminated, and the piston is fixed in the cylinder bore using specific screws and matched washers. The physical model of the churning losses test pump includes a temperature sensor, pressure sensor, outlet hole, pair of cover plates, pair of covers, pair of bearings, pair of sealing, and pair of sealing rings. A physical model of the churning losses test pump is illustrated in Figure 1.

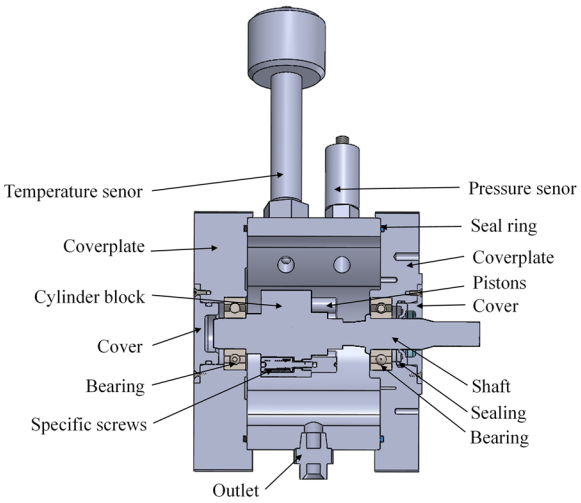

Figure 1 The physical model of the churning losses test pump

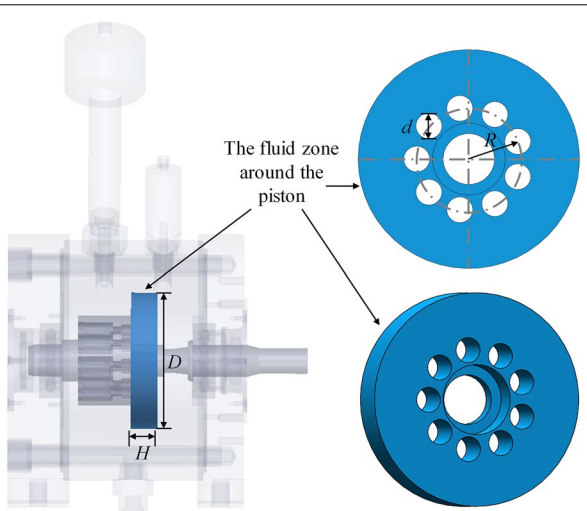

Figure 2 Fluid zone around the piston in the churning losses test pump

Because this study focuses on the effect of the number of pistons on churning losses, only the fluid zone around the piston is utilized as the research object. The number of pistons at the same speed is the only variable. At the same speed, the impact on the cylinder block is caused by the change in the number of pistons rather than the cylinder block affecting the piston. Therefore, the interaction between the piston and fluid area of the cylinder is not considered in this study. The inner wall of the test pump is round because there is no variable mechanism. The fluid zone is illustrated in Figure 2.

Considering the dynamic balance of the churning losses test pump, three, six, and nine pistons are utilized as the

research objects in this study. As illustrated in Figure 3, a CFD model of the fluid zone around the piston is extracted. Figures 3a–c illustrate the fluid zones of the three, six, and nine pistons, respectively.

The density of the hydraulic oil changes owing to cavitation, aeration, and compressibility; however, to accurately calculate churning losses and other physical phenomena that occur in axial piston pumps, these factors must be considered. Cavitation is a difficult challenge in CFD simulations, which is because the density difference between the gas and liquid is large, and the strong coupling between the gas or vapor composition and average flow makes it difficult to perform. When cavitation occurs, the general solution algorithm may not be able to handle the issue of a large liquid-gas density ratio, which may cause numerical instability. However, based on the research by Singhal et al. [27], the cavitation model can be represented by the following equation:

$$\begin{aligned}&\frac{\partial}{\partial t}\int_{V(t)}\rho f_v \mathrm{d}V+\int_S \rho[(\boldsymbol{v}-\boldsymbol{v_S})\cdot\boldsymbol{n}]f_v \mathrm{d}S\\&=\int_S\left(D_f+\frac{\mu_t}{\sigma_f}\right)(\nabla f_v\cdot\boldsymbol{n})\mathrm{d}S+\int_V(R_e-R_c)\mathrm{d}V,\end{aligned}\tag{2}$$

where V is the control volume and its enclosed surface is denoted by S, $\boldsymbol{n}$ is the normal vector of S and is pointed outward, f_v is the vapor mass fraction, $\boldsymbol{v}$ and $\boldsymbol{v_S}$ are the velocity vectors of the fluid and surface motion, respectively, D_f is the diffusivity of the vapor mass fraction, μ_t is the turbulent viscosity, and σ_f is the turbulent Schmidt number.

The vapor generation rate R_e and the vapor condensation rate R_c are given by:

$$R_e=C_e\frac{\sqrt{k}}{\sigma}\rho_l\rho_v\left[\frac{2}{3}\frac{(p-p_v)}{\rho_l}\right]^{1/2}(1-f_v-f_g),\tag{3}$$

$$R_c=C_c\frac{\sqrt{k}}{\sigma}\rho_l\rho_v\left[\frac{2}{3}\frac{(p-p_v)}{\rho_l}\right]^{1/2}f_v,\tag{4}$$

where C_e and C_c denote the cavitation evaporation and condensation coefficients, respectively, p_v is the liquid vapor pressure, k is the turbulent kinetic energy, and σ is the surface tension.

The relationship between the mass fraction f_v of the vapor and density ρ of the fluid mixture is described as follows:

$$\frac{1}{\rho}=\frac{f_v}{\rho_v}+\frac{f_g}{\rho_g}+\frac{1-f_v-f_g}{\rho_l},\tag{5}$$

where f_g is the gas mass fraction, ρ_v is the vapor density, ρ_g is the gas density, and ρ_l is the liquid density.

The turbulence models suitable for this simulation include standard k-ε, RNG k-ε, and SST k-ω models. The SST k-ω model has a high calculation accuracy solid separation on the wall. However, compared with the k-ε model, the SST k-ω model is more difficult to converge, and the calculation results are very sensitive to the initial conditions. Because the RNG k-ε model adds a condition to the e equation and considers the turbulent vorticity, the accuracy is improved compared to the standard k-ε model. The calculation time of the RNG k-ε model also increases. Considering the calculation time and accuracy, the RNG k-ε model is selected as the turbulence model for this calculation. Based on the studies of Launder et al. [28] and Yakhot et al. [29], the integral form of the RNG k-ε model can be expressed as

$$\begin{aligned}&\frac{\partial}{\partial t}\int_{V(t)}\rho k \mathrm{d}V+\int_S \rho[(\boldsymbol{v}-\boldsymbol{v_\sigma})\cdot\boldsymbol{n}]k \mathrm{d}S\\&=\int_S\left(\mu+\frac{\mu_t}{\sigma_k}\right)(\nabla k\cdot\boldsymbol{n})\mathrm{d}S+\int_V(G_t-\rho\varepsilon)\mathrm{d}V,\end{aligned}\tag{6}$$

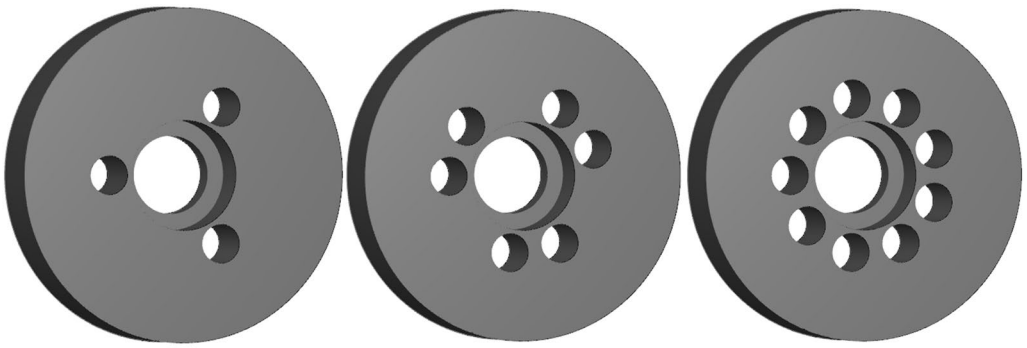

(a) Three pistons (b) Six pistons (c) Nine pistons

Figure 3 Fluid zone around the piston

$$\begin{aligned}\frac{\partial}{\partial t}\int_{V(t)}\rho\varepsilon \mathrm{d}V+\int_{S}\rho[(\boldsymbol{v}-\boldsymbol{v_S})\cdot\boldsymbol{n}]\varepsilon \mathrm{d}S\\ =\int_{S}\left(\mu+\frac{\mu_t}{\sigma_\varepsilon}\right)(\nabla\varepsilon\cdot\boldsymbol{n})\mathrm{d}S\\ +\int_{V}\left(c_1G_t\frac{\varepsilon}{k}-c_2(RNG)\rho\frac{\varepsilon^2}{k}\right)\mathrm{d}V,\end{aligned}\tag{7}$$

$$c_2(RNG)=c_2+\frac{C_\mu\eta^3\left(1-{}^{\eta}/_{\eta_0}\right)}{1+\beta\eta^3},\tag{8}$$

$$\eta=\frac{k}{\varepsilon}\sqrt{p},\tag{9}$$

where η_0 and β are hard-coded constants in Pumplinx, σ_k is the Prandtl number of the turbulent kinetic energy, σ_ε is the Prandtl number of the turbulent dissipation rate, and c_1 and c_2 are empirical constants. Their values are: η_0=4.38, β=1.92, $\sigma_k=1$, $\sigma_\varepsilon=1.3$, $c_1=1.44$, $c_2=1.92$.

The turbulent kinetic energy k is defined as:

$$k=\frac{1}{2}\left(\boldsymbol{v}'\cdot\boldsymbol{v}'\right),\tag{10}$$

where $\boldsymbol{v}'$ is the turbulent fluctuation velocity and the turbulent kinetic energy dissipation rate ε is defined as

$$\varepsilon=2\frac{\mu}{\rho}\overline{\left(S_{ij}'\cdot S_{ij}'\right)},\tag{11}$$

where the strain tensor S_{ij}' is defined as:

$$S_{ij}'=\frac{1}{2}\left(\frac{\partial u_i'}{\partial x_j'}+\frac{\partial u_j'}{\partial x_i'}\right),\tag{12}$$

where u'_i $(i=1, 2, 3)$ is the component of $\boldsymbol{v}'$, and the calculation formula of turbulent viscosity μ_t is expressed as

$$\mu_t=\rho C_\mu\frac{k^2}{\varepsilon},\tag{13}$$

where the value of C_μ is 0.09.

The turbulence generation term G_t can be expressed by the shear stress tensor and velocity as follows:

$$G_t=-\rho\overline{u_i'u_j'}\frac{\partial u_i}{\partial x_j}.\tag{14}$$

The expression of turbulent Reynolds stress is expressed as:

$$\tau_{ij}'=-\rho\overline{u_i'u_j'}.\tag{15}$$

The above equation can also be modeled using the Boussinesq approximation, as expressed below:

$$\tau_{ij}'=\mu_t\left(\frac{\partial u_i}{\partial x_j}+\frac{\partial u_j}{\partial x_i}\right)-\frac{2}{3}\left(\rho k+\mu_t\frac{\partial u_k}{\partial x_k}\right)\partial_{ij}.\tag{16}$$

According to fluid dynamics, the pressure resistance expression of a single piston can be written as [30]

$$F=\frac{1}{2}C_d\rho v_p^2dl,\tag{17}$$

where C_d is the drag coefficient, d is the piston diameter, v_p is the piston linear velocity, l is the piston length, C_d is determined by the Reynolds coefficient Re. The Reynolds coefficient Re can be expressed as [31]

$$Re=\frac{\rho v_p d}{\mu}.\tag{18}$$

When the grid is generated, the computational and boundary conditions of the CFD model are specified. The piston and shaft are set up as "rotating wall", and they rotate about the axis at the same speed. The other surfaces are set up as "wall". The pump in this test is a reversible pump with a symmetrical structure; hence, clockwise and counterclockwise rotations no effect on the research content. In this study, the rotational directions of the shaft and piston are clockwise. It is assumed that the initial state of the fluid in the flow field is stationary, and no heat conduction occurs when the piston agitates the fluid. The test pump case is communicated with the atmosphere; hence, the case pressure is set to 0.1 MPa. In this study, the case pressure is set as the reference liquid pressure. ISO VG 32 oil is utilized as the fluid medium. The geometry of the CFD model and properties of the hydraulic oil are presented in Table 1. The physical properties of the hydraulic fluids originate from Ivantysyn [32].

Table 1 Parameters for the CFD model

Description	Value	Unit
Piston diameter d	10	mm
Pitch circle radius of piston bores R	20	mm
Diameter of the fluid domain D	85	mm
Height of the fluid domain H	16.46	mm
Rotational speed of piston	500–7500	r/min
Rotational speed of shaft	500–7500	r/min
Case pressure	0.1	MPa
Fluid density	872	kg/m^3
Kinematic viscosity	32	mm^2/s
Liquid bulk modulus	1.3	GPa
Vapor pressure	10^{-3}	Pa

2.2 Grid Generation

Grid quality has a significant influence on the accuracy of numerical results. The automatic mesh generator of Pumplinx is utilized to mesh the fluid zone. The fluid zone is meshed using body-fitted binary-tree meshing. Although this mesh is not the best solution for near-wall treatment, we compensate for this weakness by encrypting the mesh. In addition, PumpLinx's solvers are re-optimized on a conventional basis; hence, the solution accuracy is higher, and requirements for near-wall mesh are not high. Therefore, Pumplinx's grid scheme is applicable in this study. A grid independence test is performed to balance the calculation time and error. Five grid schemes are designed for this study. Except for the number of grids, the other parameters of the five schemes are exactly the same. This grid-independent analysis is performed using an axial piston pump with nine pistons at 3000 r/min. Figure 4 illustrates the relationship between the torque and grid number. We can observe from the figure that the torque changes significantly when the number of grids is negligible. When the number of grids is relatively large, this fluctuation is negligible. For schemes with 170 and 210 thousand grids, the difference in torque is close to 1%. Furthermore, we observe the difference between the cavitation cloud diagrams obtained under different grid numbers. For the schemes with 30 thousand and 86 thousand grids, the cavitation cloud diagram is obviously different from that of the other grid schemes. When the number of grids exceeds hundred thousand, the cavitation cloud diagram hardly changes. Considering the computational accuracy and speed, the grid number 180 thousand was selected for the CFD simulation.

The grid of the fluid zone around the piston is illustrated in Figure 5. As illustrated in Figure 5a, there are 188078 cells, 576575 faces, and 200456 nodes in the volume grid. As illustrated in Figure 5b, there are 179806 cells, 552109 faces, and 192498 nodes in the volume grid. As illustrated in Figure 5c, there are 171534 cells, 527643 faces, and 184540 nodes in the volume grid.

2.3 Simulation Results

Figure 6 illustrates the simulation results of the variation in the torque of churning losses with the number of pistons at different rotation speeds of the axial piston pump. The simulation results revealed that the churning losses first increased and then decreased with an increase in the piston number. When the number of pistons of the axial piston pump changed from three to six at six different speeds, the churning losses increased by an average of 5.33%. When the piston number of the axial piston pump changed from six to nine at six different speeds, the churning losses reduced by an average of 6%. The axial piston pump with six pistons had the largest torque of churning losses. Figure 7 illustrates the fluid zone streamlines around the piston. The streamlines of the main streamlines of the three pistons and six pistons

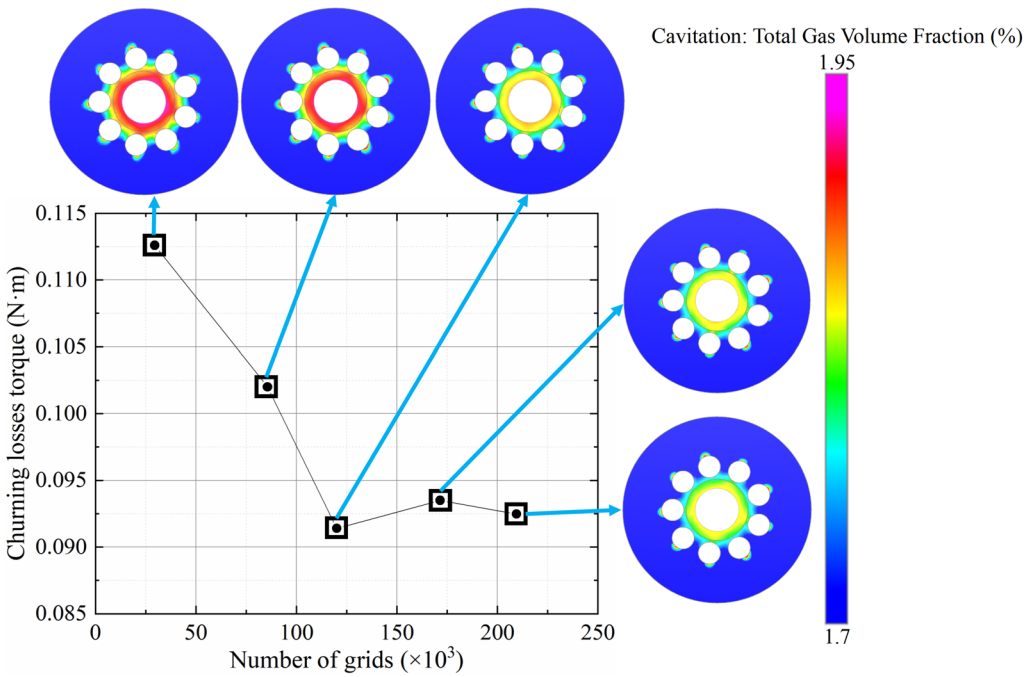

Figure 4 Torque value and cavitation degree under different grid numbers

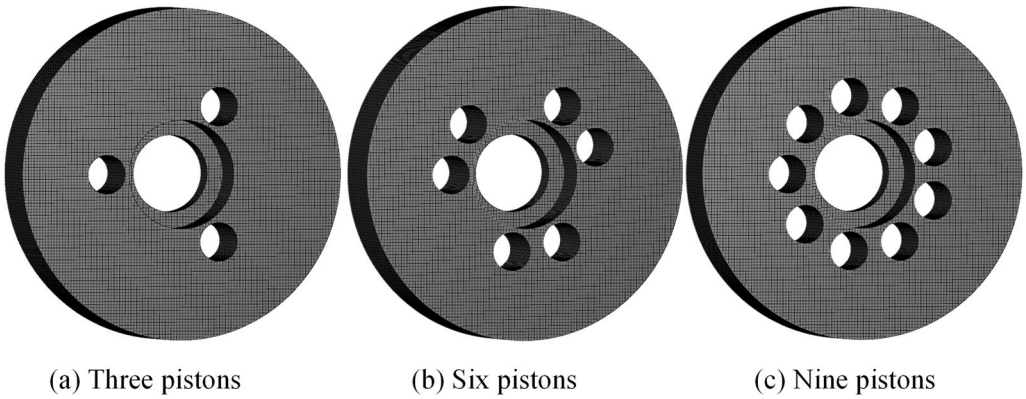

Figure 5 Grid of the fluid zone around the piston

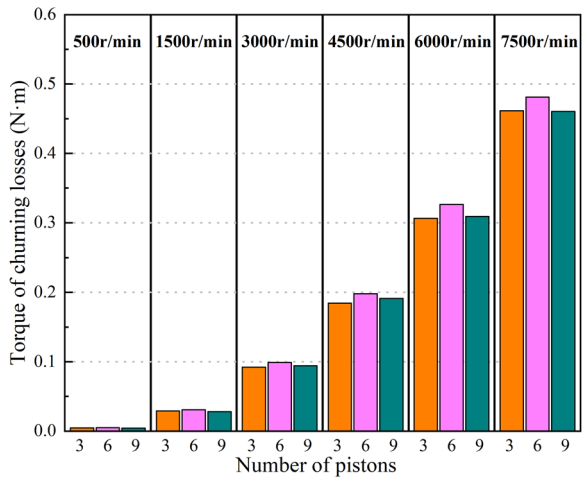

Figure 6 Simulation torque value of churning losses for different numbers of pistons

indicated a "triangular" shape. When the number of pistons increased to nine, the streamlines could be observed as two relatively isolated rings inside and outside. This is mainly because the ratio of the clearance between the multi-pistons to the piston diameter is less than one. The hydrodynamic shadowing effect becomes significant and the rotation resistance is relatively reduced. This is why the torque of the churning losses of the nine pistons is smaller than that of the six pistons.

At 1500 r/min, 3000 r/min, 4500 r/min, and 6000 r/min, the maximum gas volume fractions of the flow zone of the three pistons were 1.79%, 2.30%, 4.4%, and 34.36%, respectively. At 1500 r/min, 3000 r/min, 4500 r/min, and 6000 r/min, the maximum gas volume fractions of the flow zone of the six pistons were 1.76%, 2.06%, 2.85%, and 58.36%, respectively. At 1500 r/min, 3000 r/min, 4500 r/min, and 6000 r/min, the maximum gas volume fractions of the flow zones of the nine pistons were 1.74%, 1.99%,

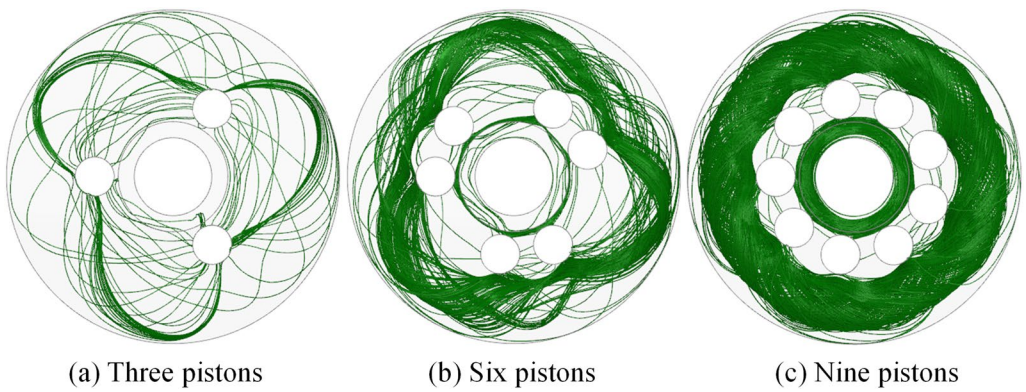

Figure 7 Streamline in fluid zone

2.51%, and 30.09%, respectively. The results indicate that the maximum gas volume fraction increased rapidly with increasing rotating speed. According to the more obvious cavitation cloud diagram of the fluid zone around the piston (Figure 8d), it can be observed that the cavitation area is mainly located around the piston. More specifically, for the cavitation areas of three and six pistons, a "propeller" shape was formed. For the cavitation region

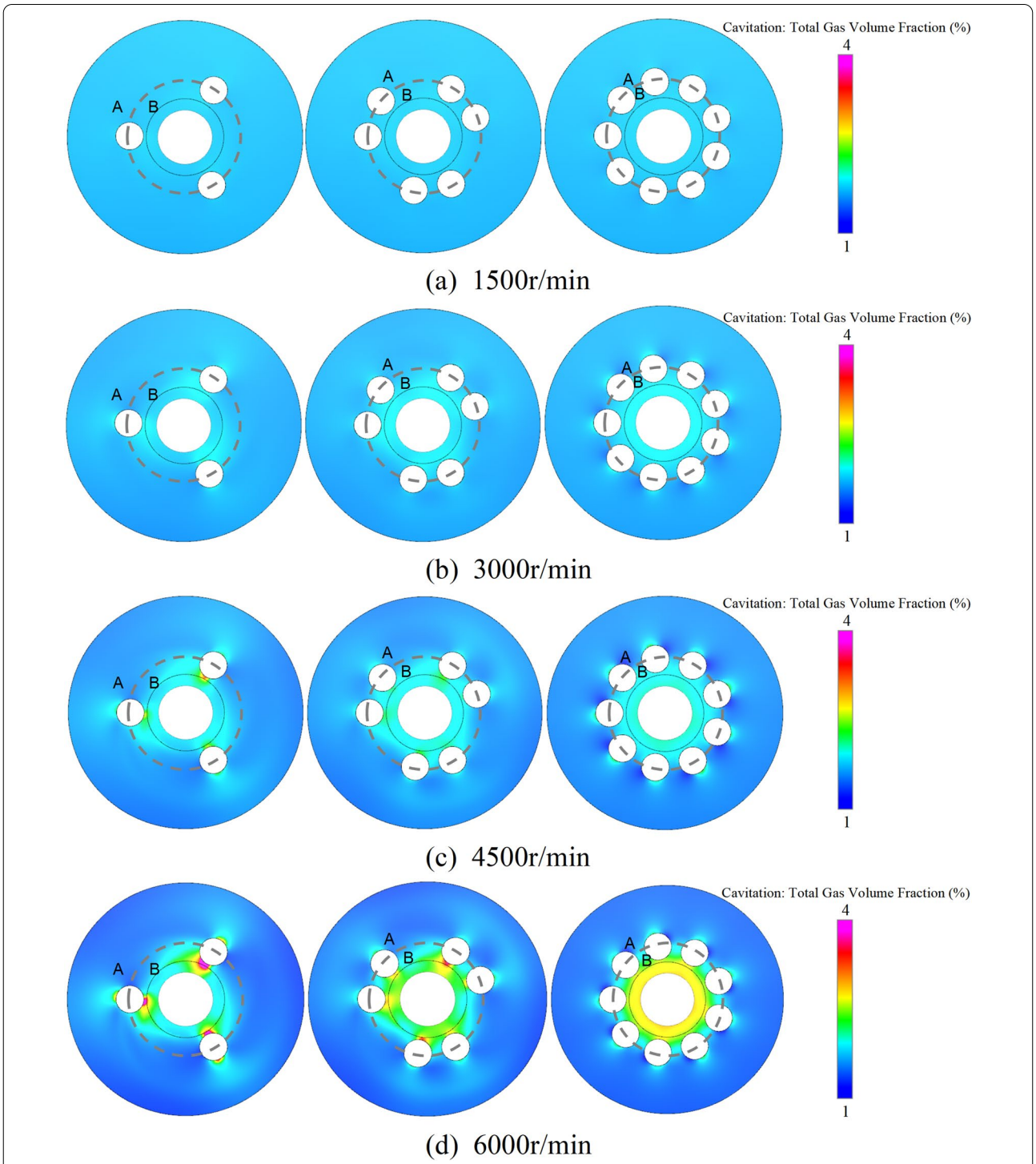

Figure 8 Cavitation cloud diagram of the fluid zone

of the nine pistons, the gas volume fraction was radial and uneven, and the total gas volume fraction in area B was much higher than that in area A in the figure. This is because of the hydrodynamic shadowing effect, and the flow in areas A and B was significantly reduced to form two relatively closed areas. The CFD simulation results of churning loss cavitation are consistent with the relevant experimental results [16].

In this study, a CFD simulation model without cavitation was established to study the influence of cavitation on churning losses. The results of the churning losses of the CFD simulation model without cavitation are illustrated in Figure 9. When the piston number of the pump increased from three to six at six different speeds, the churning losses increased by an average of 6.48%. When the piston number of the pump increased from six to nine at six different speeds, the churning losses increased by an average of 9.95%. This is different from the cavitation trend. Therefore, by comparing the simulation results, it was determined that cavitation has a significant influence on churning losses.

3 Experiments

3.1 Experimental Setup

To verify the accuracy of the CFD simulation results, a test rig was established for churning losses of the simulation pump. The churning losses test rig mainly comprised an oil tank, test pump, electric motor, sensors, electric control box, and operation console. The real object of the test rig is illustrated in Figure 10. The experimental operating conditions and test pump geometry are consistent with those of the CFD simulation model. Six piston pumps were obtained by removing three pistons from the nine piston pumps. For the three piston pumps, it was obtained by removing six pistons from the nine piston pumps. After removing the piston, the ordinary piston was replaced with a special piston. This special piston can be connected to a specific screw at the other end without sticking to the cylinder hole [16].

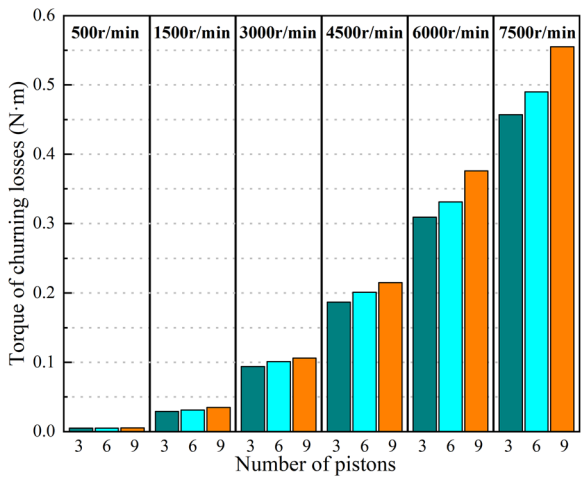

Figure 9 Simulation torque value of churning losses for different numbers of pistons without cavitation

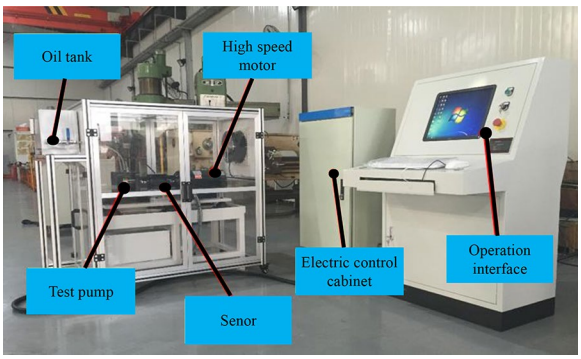

Figure 10 The churning losses test rig

The test pump was powered by a motor capable of achieving a high speed. The torque and speed of the test pump was measured using the torque/speed sensor type JN338-10AG-T. This sensor measured an ultimate speed of 16000 r/min and ultimate torque of 10 N·m with a measurement accuracy of ±0.2%. The oil temperature inside the housing was measured using a NEXON TA3000 temperature sensor with a temperature range of −50~600 °C and measurement accuracy of ±0.2%. The oil-stirring chamber in the housing was the main chamber. The pressure test sensor selected for the chamber was a Huba 520. The sensor had a built-in signal amplifier, which had high sensitivity, measurement accuracy, and long service life. The pressure sensor could measure a maximum pressure of 2.5 MPa and a measurement accuracy of ±0.3%. The details of the sensors utilized in the test rig are presented in Table 2.

The main shaft and motor were connected by a torque/speed sensor and two couplings. The main shaft was supported by a sealed ball bearing, and the friction torque of the bearing was experimentally determined. This torque was subtracted from the total torque measurement, thereby obtaining a net churning torque loss.

Table 2 Details of the sensors

Description	Detail
Torque/speed sensor	JN338, range 0–10 N·m, accuracy ±0.2%; range 0–16000 r/min
Temperature sensor	NEXON, range — 50~600 ℃, accuracy ±0.2%
Pressure sensor	Huba, range 0–2.5 MPa, accuracy ±0.3%

The torque loss of the churning was obtained by calculating the torque difference between the "wet casing" and "dry casing". Because it is difficult to measure the churning losses during the start-up stage of the piston pump, all the torque values in this study were measured when the system was stable. The experimental torque of the churning loss M_c can be expressed as:

$$M_c = M_w - M_d, \tag{19}$$

where M_w is the torque value of the shaft in the "wet casing" and M_d is the torque value of the shaft in the "dry casing".

Using this method, the torques of the churning losses of different parts can be calculated. The torque of the churning losses generated by the cylinder M_{cc} is as follows:

$$M_{cc} = M_{wcc} - M_{dcc}, \tag{20}$$

where M_{wcc} is the torque value of the cylinder acting on the shaft in the "wet casing" and M_{dcc} is the torque value of the cylinder acting on the shaft in the "dry casing".

It is required that the piston rotates with the cylinder block, and the fluid between the piston and cylinder clearly interacts. However, in this study, the piston was the only variable at the same speed. The change in the churning losses of the cylinder was caused by the change in the number of pistons; therefore, the torque of the churning losses generated by the piston M_{cp} is as follows:

$$\begin{aligned} M_{cp} &= M_{ccp} - M_{cc} \\ &= (M_{wccp} - M_{dccp}) - (M_{wcc} - M_{dcc}) \\ &= M_{wccp} - M_{dccp} - M_{wcc} + M_{dcc}, \end{aligned} \tag{21}$$

where M_{ccp} is the experimental torque of churning losses due to the cylinder and piston, M_{wccp} is the torque that the cylinder and piston act on the main shaft in the "wet casing", and M_{dccp} is the torque that the cylinder and piston act on the main shaft in the "dry casing".

The churning losses test rig realized an experimental measurement of the churning losses of the rotating parts of the pump. The main structure is illustrated in Figure 11. By arranging grease-lubricated bearings with stable friction performance, the interference of the friction torque at the bearings on the measurement of the churning losses was eliminated. In addition, to avoid changes in the hydraulic oil parameters, the temperature of the hydraulic oil was maintained at 35 °C and oil pressure was maintained at 0.102 MPa during operation. The test pump considered all the factors that affect churning losses and eliminated the interference of other power losses in the pump during the churning losses test. Via the experimental device, an experimental study of the change in the churning losses with the rotation speed and piston can be conveniently conducted.

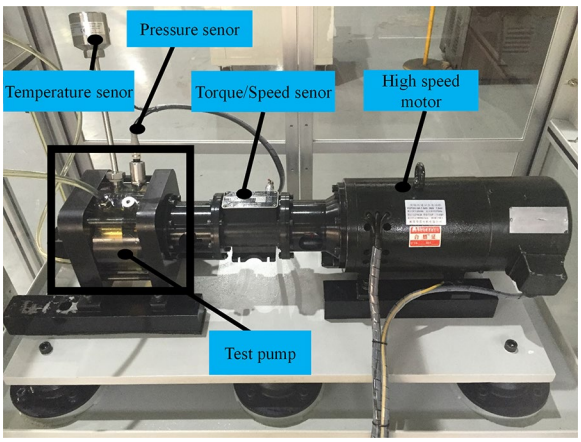

Figure 11 The main structure of the churning losses test rig

3.2 Test Results

In this study, the average churning losses were obtained by repeated tests on the test rig. Figure 12a illustrates the experimental and simulation results of the torque of the churning losses with the number of pistons at different axial piston pump speeds. Figure 12b illustrates the experimental and simulation results of the power of the churning losses with the number of pistons at different axial piston pump speeds.

From the test curve, it can be observed that with an increase in the number of pistons, except for the rotation speed of 1500 r/min, the torque of the churning losses first increased and then decreased. The axial piston pump with six pistons had the largest torque of churning losses. There were a few errors between the experimental and simulation results, but the overall trend was consistent. By comparing the average torque of the churning losses of the three piston pumps at different speeds, it can be calculated that the experimental value is 15.2% larger than the simulated value. Similarly, we can calculate that the experimental value of the six piston pumps is 18.5% larger than the simulated value, and experimental value of the nine piston pumps is 18.2% larger than the simulated value. In this study, an additional control group of the non-cavitation model was added to determine the influence of the cavitation model on churning losses. By comparing the simulation values of churning losses with and without cavitation, it was determined that non-cavitation is generally greater than cavitation. Moreover, regarding nine pistons, the churning losses in the case of no cavitation were significantly greater than those in the case of cavitation.

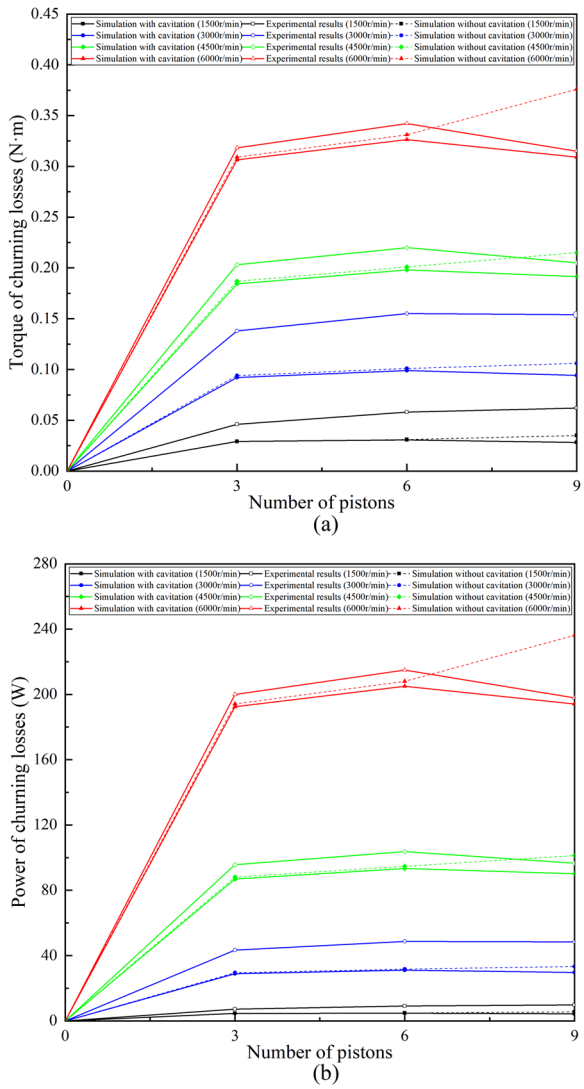

Figure 12 Comparison of experimental results and simulation results: **a** torque of churning losses, **b** power of churning losses

This also led to the fact that the churning losses under non-cavitation conditions altered with the number of pistons, which was obviously different from the experiment. This is mainly because cavitation around the piston generates air, and the piston changes from a state of stirring in the oil to a state of stirring in the oil and gas mixture. The cavitation caused by churning losses is illustrated in Figure 13. Because the accuracy of the simulation model improved after cavitation, the influence of cavitation must be considered. As illustrated in Figure 12b, at the same rotation speed, the law of the power of the churning losses changing with the piston is basically the same as the torque of the churning losses. However, when the piston number is the same,

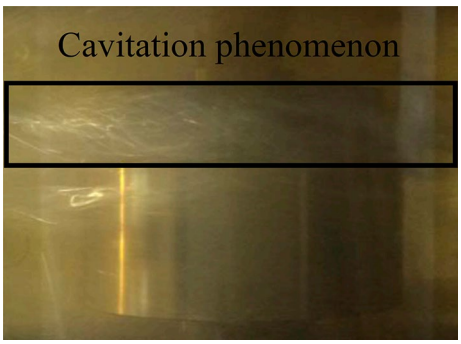

Figure 13 Cavitation in experiments

the power of the churning losses increases exponentially with increasing speed. This indicates that at high speeds, the churning loss caused by the piston must be considered. Because this CFD simulation ignores the difference in the internal fluid chamber of the irregular housing in the test pump and does not analyze the effect of the oil flow state around the cylinder on the oil flow state around the piston, it will cause some errors. Parts of the test process, data processing, and analysis process will produce errors, which may affect the results of churning losses. However, it can be determined that the error percentage between the experimental and simulation values decrease gradually with the increase in rotating speed. This is because the air ring generated around the multi-pistons under high-speed conditions makes the influence of the casing and cylinder negligible; hence, the error also becomes relatively smaller. Therefore, when comparing the test results with the simulation results, it can be determined that although there are a few errors, the test results are basically consistent with the simulation conclusions.

4 Discussion

The previous analysis results indicate that as the number of pistons increases, the churning losses first increase and then decrease; however, seven piston pumps commonly utilized in engineering have not been studied. Therefore, in this study, we compared seven and nine piston pumps at the same displacement. The displacement calculation formula of the axial piston pump is given by

$$V_p = \frac{\pi d^2}{2} z R \tan\gamma, \tag{22}$$

where V_p denotes the displacement, γ denotes the swash plate angle, and z denotes the piston number. To ensure that the displacements of the seven and nine piston pumps are the same, the piston diameter d, pitch circle radius of piston bores R, and swash plate angle γ can be

Table 3 Geometric parameters of pumps with the same displacement

Geometric parameters	9 pistons	7 pistons (1)	7 pistons (2)	7 pistons (3)
d (mm)	10	10	10	12.86
R (mm)	20	25.7	20	20
γ (°)	14.5	14.5	18.4	14.5

altered. The geometric parameters of pumps with the same displacement are presented in Table 3.

The three-dimensional model of the fluid zone drawn according to the geometric parameters in Table 3 is illustrated in Figure 14.

According to the previous method, we conducted a CFD simulation research on pumps with seven pistons with different parameters. Figure 15 illustrates the torque results for the churning losses of different pumps with the same displacement. Under the same displacement, pumps with seven pistons have greater churning losses than pumps with nine pistons. After further studying the three parameters of the seven piston pumps, it can be determined that the pitch circle radius R has a much greater influence on the churning losses than the other two parameters. Although the angular velocity ω of the piston is the same, the linear velocity v_p increases with the pitch circle radius R by 28.5%. According to Eq. (17), it can be determined that the pressure resistance of a single piston is proportional to the square of the linear velocity v_p. This is why pitch radius R has a significant influence on the churning losses.

5 Conclusions

In this study, the relationship between the number of pistons and churning losses was mainly studied using CFD simulation. Subsequently, to verify the feasibility of the CFD simulation, a churning loss test rig was established.

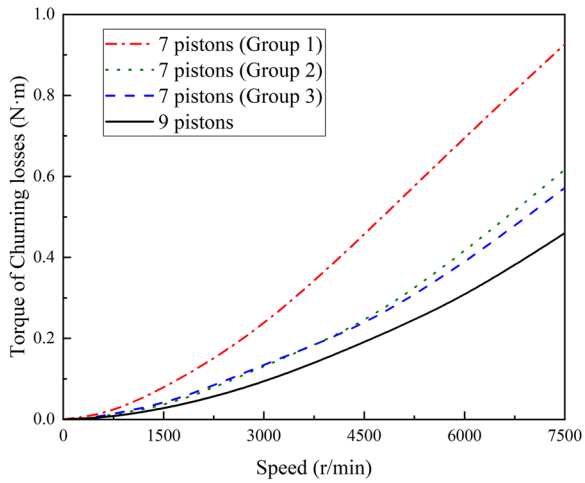

Figure 15 Comparison of the torque results of churning losses of the pump with the same displacement

We also compared the churning losses of seven and nine piston pumps with the same displacement. Based on an analysis of the simulation and experimental results, the following conclusions can be drawn:

(1) When the speed is the same, the number of pistons increases, torque of the churning losses first increases and then decreases, while the axial piston pump with six pistons has the largest torque of churning losses. The main reason is that the hydrodynamic shadowing effect becomes increasingly obvious with an increase in piston number, and this leads to a reduction in churning losses to a certain extent.

(2) The cavitation phenomenon is conducive for the reduction of churning losses, particularly under high-speed conditions. The cavitation area of the axial piston pump is mainly concentrated around

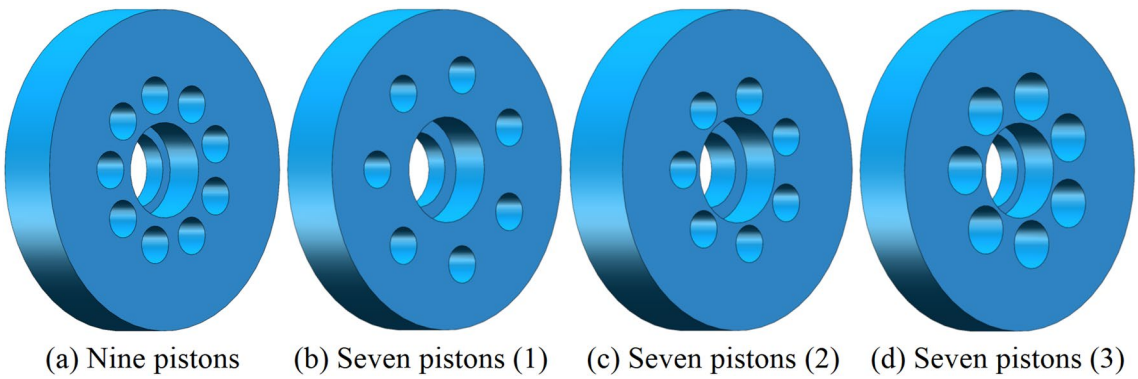

Figure 14 Three-dimensional model of the fluid zone

the piston, and cavitation becomes increasingly serious as the speed increases.

(3) At the same displacement, the churning losses of the nine pistons are significantly less than those of the seven pistons. Under the condition of the same piston and displacement, the pitch circle radius of the piston bores has the greatest influence on the churning losses. By reducing the pitch circle radius of the piston bores, churning losses can be significantly reduced.

The results of this study have certain guiding significance for the structural design and model selection of axial piston pumps. However, in the process of building the CFD simulation model, the influence of the cylinder block on the actual pump was ignored, and the difference in the extension length of the piston was not considered. Considering the continuity of the research topics, in future studies, we will consider the influencing factors, such as the cylinder block and extension length of the piston.

Acknowledgements
Not applicable.

Authors' Information
Ying Li, born in 1992, is currently a lecturer at *Yanshan University, China*. She received her Ph.D. degree from *Zhejiang University, China*, in 2019. Her research interests include energy losses and work efficiency of hydraulic pumps/motors, fluid power components, and systems.
Xing Chen, born in 1998, is currently a Master candidate at *School of Mechanical Engineering, Yanshan University, China*.
Hao Luo, born in 1998, is currently a Master candidate at *School of Mechanical Engineering, Yanshan University, China*.
Junhui Zhang, born in 1983, is currently deputy director at *State Key Laboratory of Fluid Power Transmission and Control, Zhejiang University, China*. His research interests include fluid power transmission and control, and hydraulically driven robots.
Jin Zhang, born in 1984, is currently an associate professor and Ph.D. candidate supervisor at *School of Mechanical Engineering, Yanshan University, China*. His main research interests include high-performance hydraulic component development and flow-field visualization analysis.

Author Contributions
YL supervised the entire trial, XC and HL wrote the manuscript, and JHZ and JZ assisted with sampling and laboratory analyses. All authors read and approved the final manuscript.

Funding
Supported by National Natural Science Foundation of China (Grant No. 52005429), Open Foundation of State Key Laboratory of Fluid Power and Mechatronic Systems of China (Grant No. GZKF-201911), and National Key Research and Development Program of China (Grant No. 2018YFB2000703).

Competing Interests
The authors declare no competing financial interests.

Author Details
[1]School of Mechanical Engineering, Yanshan University, Qinhuangdao 066004, China. [2]State Key Laboratory of Fluid Power Transmission and Control, Zhejiang University, Hangzhou 310027, China.

Received: 12 April 2021 Revised: 28 May 2022 Accepted: 1 June 2022
Published online: 28 June 2022

References

[1] B Xu, Y Chen, J H Zhang. Current researches and progress on vibration and noise reduction technology of axial piston pump. *Chinese Hydraulics & Pneumatics*, 2014, 3(3): 1-12. (in Chinese)
[2] H Y Yang, B Zhang, B Xu. Development of axial piston pump/motor technology. *Journal of Mechanical Engineering*, 2008, 44(10): 46–47. (in Chinese)
[3] S G Ye, J H Zhang, B Xu, et al. Experimental studies of the vibro-acoustic characteristics of an axial piston pump under run-up and steady-state operating conditions. *Measurement*, 2019, 133: 522-531.
[4] S G Ye, J H Zhang, B Xu. Noise reduction of an axial piston pump by valve plate optimization. *Chinese Journal of Mechanical Engineering*, 2018, 31: 57.
[5] L A Bronshteyn, J H Kreiner. Energy efficiency of industrial oils. *Tribology Transactions*, 1999, 42(4): 771-776.
[6] M D Gao, H H Huang, X Y Li, et al. A novel method to quickly acquire the energy efficiency for piston pumps. *Journal of Dynamic Systems, Measurement, and Control*, 2016, 138(10): 101004.
[7] H S Jeong, H E Kim. A novel performance model given by the physical dimensions of hydraulic axial piston motors: Experimental analysis. *Journal of Mechanical Science and Technology*, 2007, 21(4): 83-97.
[8] B Zhao, W Guo, L Quan. Cavitation of a submerged jet at the spherical valve plate/cylinder block interface for axial piston pump. *Chinese Journal of Mechanical Engineering*, 2020, 33: 67.
[9] H Murrenhoff, U Piepenstock, T Kohmäscher. Analysing losses in hydrostatic drives. *Proceedings of the JFPS International Symposium on Fluid Power*. Toyama, Japan, September 15-18, 2008: 103-108.
[10] N D Manrin. *Torque on the cylinder block of an axial-piston swash-plate type hydrostatic pump*. Des Moines: Iowa State University, 1996.
[11] D McCandlish, R E Dorey. The mathematical modelling of hydrostatic pumps and motors. *Proceedings of the Institution of Mechanical Engineers, Part B: Management and engineering manufacture*, 1984, 198(3): 165-174.
[12] D S Jang. *Verlustanalyse an axialkolbeneinheiten*. Aachen: RWTH Aachen University, 1997.
[13] Parker Hannifin Corporation. *Added power for saw motors. Trollhattan, Vastergotland*: Parker Hannifin Manufacturing Sweden AB, 2021[2022-04-20]. https://www.parker.com/Literature/PMDE/Sales_Marketing/Fixed_Motors/MSG30-8255-B1_UK.pdf.
[14] C P Enekes. *Ausgewählte maßnahmen zur effizienzsteigerung von axialkolbenmaschinen*. Aachen: RWTH Aachen University, 2012.
[15] M Zecchi, A Mehdizadeh, M Ivantysynova. A novel approach to predict the steady state temperature in ports and case of swash plate type axial piston machines. *Proceedings of the 13th Scandinavian International Conference on Fluid Power*, Linköping, Sweden, June 3-5, 2013: 177-187.
[16] J H Zhang, Y Li, B Xu, et al. Experimental study on the influence of the rotating cylinder block and pistons on churning losses in axial piston pumps. *Energies*, 2017, 10(5): 662.
[17] D Hasko, L Z Shang, E Noppe. Virtual assessment and experimental validation of power loss contributions in swash plate type axial piston pumps. *Energies*, 2019, 12(16): 3096.
[18] H S Jeong, H E Kim. On the instantaneous and average piston friction of swash plate type hydraulic axial piston machines. *KSME International Journal*, 2004, 18(10): 1700-1711.
[19] V S Mehta, N D Manring. Torque ripple attenuation of an axial piston pump by continuous swash plate adjustment. *Proceedings of ASME 2005 International Mechanical Engineering Congress and Exposition*. Orlando, USA, November 5-11, 2005: 147-155.
[20] L Chen, S Ye, Z Chang, et al. Simulation research on the revolution-pressure performance of an aeronautical hydraulic axial piston pump. *Proceedings of the 2016 IEEE International Conference on Aircraft Utility Systems*, Beijing, China: IEEE, 2016: 1247-1251.
[21] C Ling, Y Q Wei, X L Zhao, et al. Design and analysis of new type of piston pump. *Journal of Southwest Jiaotong University*, 2018, 53(3): 602–609. (in Chinese)

[22] M A Asghar, Y Liu, J Cui, et al. Investigation of unsteady flow interactions in a transonic high pressure turbine using nonlinear harmonic method. *Energies*, 2018, 11(2): 342.
[23] P R Spalart. Philosophies and fallacies in turbulence modeling. *Progress in Aerospace Sciences*, 2015, 74: 1-15.
[24] Y Tao, S Q Yuan, J R Liu, et al. Influence of cross-sectional flow area of annular volute casing on transient characteristics of ceramic centrifugal pump. *Chinese Journal of Mechanical Engineering*, 2019, 32: 4.
[25] D H Wu, Y Ren, J G Mou, et al. Unsteady flow and structural behaviors of centrifugal pump under cavitation conditions. *Chinese Journal of Mechanical Engineering*, 2019, 32: 17.
[26] W Dong, W L Chu. Numerical investigation of the fluid flow characteristics in the hub plate crown of a centrifugal pump. *Chinese Journal of Mechanical Engineering*, 2018, 31: 64.
[27] A K Singhal, M M Athavale, H Y Li, et al. Mathematical basis and validation of the full cavitation model. *Journal of Fluids Engineering*, 2002, 124(3): 617-624.
[28] B E Launder, D B Spalding. The numerical computation of turbulent flows. In: *Numerical Prediction of Flow, Heat Transfer, Turbulence and Combustion*. Pergamon, 1983: 96-116.
[29] V Yakhot, S A Orszag, S Thangam, et al. Development of turbulence models for shear flows by a double expansion technique. *Physics of Fluids A: Fluid Dynamics*, 1992, 4(7): 1510-1520.
[30] C K Batchelor, G K Batchelor. *An introduction to fluid dynamics*. Cambridge: Cambridge University Press, 2000.
[31] A Roshko. Experiments on the flow past a circular cylinder at very high Reynolds number. *Journal of Fluid Mechanics*, 1961, 10(3): 345-356.
[32] J Ivantysyn, M Ivantysynova. *Hydrostatic pumps and motors: principles, design, performance, modelling, analysis, control and testing*. New Delhi: Tech Books International, 2003.